JOURNAL OF MATERIALS RESEARCH AND TECHNOLOGY 2023;23:379–390

Available online at www.sciencedirect.com

jmr&t Journal of Materials Research and Technology

journal homepage: www.elsevier.com/locate/jmrt

Original Article

Stimuli-responsive piezoelectricity in electrospun polycaprolactone (PCL)/Polyvinylidene fluoride (PVDF) fibrous scaffolds for bone regeneration

Elham Bagherzadeh [a,***], *Zahra Sherafat* [a,*], *Seyed Mojtaba Zebarjad* [a], *Azin Khodaei* [b], *Saber Amin Yavari* [b,**]

[a] *Department of Materials Science and Engineering, School of Engineering, Shiraz University, Shiraz, Iran*
[b] *Department of Orthopedics, University Medical Center Utrecht, Utrecht, the Netherlands*

ARTICLE INFO

Article history:
Received 20 November 2022
Accepted 2 January 2023
Available online 4 January 2023

Keywords:
Piezoelectric scaffold
Polymers crystallization
Fibrous composite
Bone regeneration

ABSTRACT

Polymeric scaffolds are a determinant part of modern tissue engineering owing to their great diversity, adaptability, and processability. Interestingly, the physical properties of these scaffolds, e.g., porosity, mechanical properties, and biocompatibility, can be tuned to make them smart and stimuli-responsive. In this regard, piezoelectric materials can be applied to stimulate bone regeneration by converting mechanical impulses to electrical signals. In the present research, fibers made of various blend ratios of polyvinylidene fluoride (PVDF)/polycaprolactone (PCL) were fabricated, investigated and optimized to promote bone regeneration. Uniform fibers containing β-phase PVDF were obtained due to the simultaneous stretching and high voltage applied during electrospinning. Furthermore, components interaction, crystallinity, and piezoelectric behavior were estimated through fourier-transform infrared spectroscopy (FTIR), differential scanning calorimetry (DSC), and piezometery, respectively. The samples showed improved wettability and controlled biodegradability, and the piezoelectric charge output reached up to 7.5 pC/N in the sample containing 70 wt% PVDF. At the same time, these scaffolds could provide mechanical properties close to the native bone tissue relying on the PVDF component. In vitro assessments demonstrated that the composite scaffolds were biocompatible and could support cell attachment and proliferation. Moreover, their piezoelectric behavior promoted stem cell differentiation into osteoblasts. Considering the obtained results, the potential of piezoelectric PVDF/PCL blend fibers for bone scaffolds is indisputable.

* Corresponding author.
** Corresponding author.
*** Corresponding author.
E-mail addresses: elham.bagherzadeh@shirazu.ac.ir (E. Bagherzadeh), zsherafat@shirazu.ac.ir (Z. Sherafat), S.AminYavari@umcutrecht.nl (S. Amin Yavari).

https://doi.org/10.1016/j.jmrt.2023.01.007

1. Introduction

Bone regeneration, the finely-tuned cellular and molecular events of bone reconstitution, is mandated for ongoing bone remodeling during adulthood as well as bone healing in pathological circumstances like trauma-mediated extensive defects [1]. During the last decade, engineered biomaterials with certain traits have shown tremendous potential in supporting bone regeneration in preclinical and clinical investigations [2]. For instance, extreme traumatic bone injuries may benefit from the hosting of osteogenic or stem cells by porous polymeric scaffolds, promoting the production of extracellular matrix (ECM) components and supporting proper signaling pathways between the cells and ECM [3]. However, to actively govern diverse facets of bone regeneration, the function of biomaterials as bone grafts has extended dramatically beyond their original role as passive templates [4–6]. Intriguingly, incorporating electrical stimulations using innovative conductive or piezoelectric bioimplants propelled bone tissue engineering treatments into the next step [7,8]. Due to their inherent structural asymmetry, biological molecules (e.g., amino acids and collagen) and minerals (e.g., hydroxyapatite) endow bone tissue with piezoelectric capability (i.e., to generate an electric charge due to applied mechanical tension) as a stimulatory signal for osteogenic differentiation and bone regeneration; hence, a suitable interim alternative should likewise supply similar qualities [9,10].

Recently, tailoring the properties of already-approved biomaterials to a specific bio-application has drawn much interest [11,12]. Polycaprolactone (PCL), a biocompatible polyester, has long been utilized for manufacturing three-dimensional scaffolds in bone tissue engineering [13]. Regarding its approval for biomedical applications, ease of access, stability under ambient conditions, and adjustable physicochemical properties, PCL is currently the subject of intensive research to evolve innovative and efficient bioimplants facilitating the process of bone healing [13,14]. Incorporating natural or synthetic polymers into PCL, for instance, has been shown to improve its electrical and mechanical strength, biological functions, and biodegradability [15,16]. With this in mind, diverse PCL-based polymer blends have been employed in developing bone regeneration scaffolds [17,18]. Polymer blending is a versatile and beneficial approach for developing novel materials meeting the requirements for safe and successful biological applications [19]. Moreover, the intimate interaction between polymers in blends gives better control over their properties and provides more uniform structures with fewer complexities in the fabrication process [20]. One such approach may include blending PCL with stimuli-responsive agents to form composites, such as smart piezoelectric polymer-based materials, that are easily processable and responsive to external mechanical and electrical impulses [21].

The piezoelectricity in polymers originates from their asymmetrical charge balance and structure. In polyvinylidene fluoride (PVDF), which has the highest piezoelectric properties among polymers, the relative arrangement of electronegative -CF_2 and electroactive -CH_2 groups gives five different phases, among them, piezoelectricity can be found in the polar β and γ phases, with non-symmetrical TTTT and TTTGTTTG' chain conformations (T-trans, G-gauche$^+$, G′-gauche$^-$), respectively [22,23]. To achieve the highest piezoelectric properties, some strategies should be employed to promote the phase conversion of the thermodynamically stable α phase to the piezoelectric β phase. For this purpose, methods like adding nucleating agents to the primary PVDF solution, stretching, and employing electric fields have been reported before [24–27]. Further, the last two methods coexist in the electrospinning procedure, in which the polymer solution is stretched out of a small needle in the presence of a strong electric field; thus, a high efficiency of α to β phase transformation is attainable [28,29]. Moreover, electrospun fibers as scaffolds with large surface area provide structural resemblance to the native bone ECM [30].

Considering the piezoelectric property of PVDF, it may help to overcome the drawbacks associated with the insufficient electrical properties and mechanical strength of PCL scaffolds; however, few reports have explored the impact of PVDF/PCL blends in tissue regeneration. The early attempts on this subject focused on the temperature-dependent phase behavior of the PVDF/PCL blends [31]. More than two decades later, the isothermal crystallization of PCL in PVDF/PCL heat-treated cast films and morphology of PVDF/PCL-block-poly(dimethylsiloxane) (PDMS)-block-PCL blends were explored to deepen the knowledge of the phase behavior and crystallization phenomenon in these systems [32,33]. Despite the simplicity of solution casting for preparing blend samples, the resulting films are not suitable for scaffold preparation since they cannot provide the porous structure required for proper cell/environment interaction [34]. Lately, Cheng et al. developed solution-cast PVDF/PCL films as nerve scaffolds and artificially induced micro- and macro-porosity by immersing the sample in an ethanol bath and puncturing with needles to improve the nerve regeneration capability of blend scaffolds [34]. However, the major electroactive phase in cast PVDF film samples is the γ phase, which has a lower dipole moment and electrical polarity than the β-phase [23,34]. This is while electrospun PVDF fibers are highly porous, have a remarkable surface-to-volume ratio, and include a dominant percentage of β-phase PVDF, making them suitable candidates for producing PCL/PVDF blends as scaffolds [28,35]. In this regard, Hanumantharao et al. demonstrated that core/sheath nanofiber scaffolds made by electrospinning a mixture of PCL and polyaniline (PANI), and PVDF polymers remarkably mimicked the natural anisotropy of extracellular matrix (ECM) by allowing cardiomyoblasts to align, penetrate, and proliferate across the whole scaffold surface area without the addition of any chemical factor [36]. In another study, basic fibroblast growth factor (bFGF) incorporated PVDF/PCL co-electrospun nanofibers were prepared, and their biological properties were studied. The nanofibers sustained the survival and multiplication of pluripotent stem cells and improved their osteogenic differentiation potential [37]. To the best of our knowledge, the physical, mechanical, biological, and structure-related piezoelectricity of blend PVDF/PCL fibers has not been explored yet. Herein, it is aimed to fill this gap by electrospinning the blend solutions of PCL and PVDF polymer with different ratios to grant piezoelectricity to the scaffolds. The focus of the present research is to provide in-depth

knowledge of the underlying structural changes and mechanisms that alter the piezoelectric properties and introduce PVDF/PCL blend fibers as a potential material for bone tissue engineering.

2. Experimental procedures

2.1. Materials and methods

PVDF (Kynar® 761, molecular weight (MW) = 300,000 −400,000 Da) powder was provided by Arkema. PCL, with an average MW of 80,000 Da, was purchased from Aldrich company. Dimethyl formamide (DMF, Merck, Germany) was utilized as the solvent. A 20 wt% solution of PVDF in DMF was developed and stirred at 60 °C for 1 h. Certain amounts of PCL pellets were also dissolved in DMF and stirred at 60 °C for 1 h to produce a series of solutions with 9.2, 11.7, and 13.3 wt% concentrations. For composite samples, appropriate amounts of PVDF solution were added to each of the above PCL solutions and stirred for 2 h yielding PVDF:PCL ratios of 70:30, 50:50, and 30:70, respectively, with final concentrations, kept constant at 14.8 wt%. Thereafter, 5 mL plastic syringes (22-gauge) were charged with blend solutions and placed in a horizontal electrospinning setup. The solutions were accelerated towards a ground collector rotating at 100 rpm, with fixed voltage (17 kV) and needle tip-to-collector distance (10 cm), and fed into the electric field at rates of 0.2–0.6 mL/h to obtain high-quality fibers. Samples with more PVDF content require a higher feeding rate to prevent the electrospraying of the feed solution. The produced fibers were gathered on an aluminum foil covering the collector.

2.2. Characterization

A TESCAN-Vega 3 scanning electron microscope with an accelerating voltage of 20 kV was employed for morphology observations. The evaluation of existing functional groups and bonds was conducted using a fourier-transform infrared spectroscopy (FTIR) spectrometer (ATR-FTIR Tensor II, Bruker, Germany) in a 4000-400 cm^{-1} spectrum. Thermal properties were recorded using a differential scanning calorimetry (DSC, TA, Q100) with a heating rate of 10 °C/min under nitrogen. For determining the piezoelectric properties, a tapping load of 2 N was applied to the surface of samples at a frequency of 5 Hz, and the piezoelectric charge output was measured using a piezometer (Piezo Test UI, Iran). The water wettability of the fibers was evaluated by a contact angle goniometer and tensiometer (CAG10, Jikan, Iran), and the water contact angle of a 5 μl water drop was gauged using the ImageJ software. Finally, a tensile test instrument (GOTECH, Al-3000-U, Taiwan) was used to assess the mechanical characteristics of the prepared samples at a crosshead speed of 10 mm/min.

2.3. Cell culture and in-vitro cell studies

The fabricated scaffolds were soaked in ethanol for 30 min, then washed with phosphate-buffered saline (PBS) solution, and finally exposed to UV irradiation for another 30 min to ensure complete sterilization. To conduct cell studies, 1×10^4 human mesenchymal stem cells (hMSC) were seeded on each sample in the osteogenic media (α-minimum essential medium (MEM), 10% heat-inactivated-fetal bovine serum (HI-FBS), 0.2 mM L-ascorbic acid-2-phosphate, 1% penicillin/streptomycin (Pen/Strep), 10 mM β-glycerophosphate, and 10 nM dexamethasone) in 96-well plates. Metabolic activity of the seeded cells was measured using Alamar blue assay after 1, 3, 7, and 14 days. For this purpose, seeded samples were incubated in α-MEM medium supplemented with 0.011 mg/mL resazurin salt for 2 h, and the fluorescent intensity of the collected samples was determined at excitation/emission wavelengths of 570/620 nm using a Clariostar plate reader (BMG LABTEC, Germany). The DNA content was also quantified after 14 days using a Quant-iT™ PicoGreen® dsDNA (Thermo Fisher Scientific, USA) kit according to the manufacturer's instruction. After being collected and rinsed with PBS solution, samples were lysed by adding 200 μL of lysis buffer (0.2% triton-100 in PBS) to each sample and incubating them for 30 min at room temperature. The samples were then subjected to three freeze-thaw cycles (−80 °C and RT).

As an indicator of osteoblastic activity, in the alkaline phosphatase (ALP) assay, the ability of cultured cells to convert para-nitrophenyl phosphate (pNPP) to para-nitrophenol (pNP) by ALP enzyme was measured after 7 days. After washing the scaffolds with PBS, 200 μL lysis buffer was added to each sample and incubated for 30 min at room temperature. For ALP measurement, 50 μL of pNPP solution was added to each well containing 50 μL of the cell lysate. The absorbance was determined at 405 nm with a microplate spectrophotometer. The rest of the cell lysate underwent 3 freeze-thaw cycles (−80 °C and RT) for complementary picogreen assay. The ALP activity was normalized to the DNA count determined by the picogreen assay.

Staining techniques were utilized to observe adherent cells on the scaffolds. Samples were washed with PBS and fixed with 4% formaldehyde solution at room temperature. Before staining, cells were permeabilized by treating with 0.2% Triton in PBS solution for 15 min and then washed with PBS. The 4′,6-diamidino-2-phenylindole (DAPI) and phalloidin were engaged for staining cell nuclei and cytoskeleton, respectively. Fluorescence images of cells were taken recruiting a confocal fluorescence microscope (Leica SP8X, Germany) after 1 and 7 days of cell culture. Quantitative cell studies were repeated three times, and analysis of variances (ANOVA) was used to determine meaningful variations, where p-values less than 0.05 was assumed statistically significant.

The bioactivity of scaffolds was assessed using microscopy techniques. Samples (1 cm^2) were soaked in 12 mL of simulated body fluid (SBF) solution for 4 weeks, gently washed with distilled water, dried at room temperature, and used for scanning electron microscopy (SEM) observation [38].

In vitro degradation studies were performed according to the ASTM F1635 method. Briefly, 2 cm^2 fibrous samples were cut, weighed, and immersed in 10 mL PBS solution for specific periods of 1, 4, 7, 14, 28, and 56 days. Each experiment was repeated three times. After each time point, the sample was rinsed with distilled water thoroughly, dried at room temperature, and weighed to obtain the degraded sample weight. The initial and final sample weights were used to calculate the degradation percentage of each sample.

3. Results and discussion

3.1. Morphological and structural assessment

As described earlier, the prepared blend solutions of different compositions and pure PVDF and PCL solutions were electrospun. The cloudy appearance of the blend solutions indicated that the components were mostly immiscible; nevertheless, no visible phase separation occurred in the solutions for at least 3 h [39]. The electrospinning solution was replaced every 2.5 h to prevent possible inhomogeneity in the fibers. As illustrated in the electron micrographs (Fig. 1a–e), all fabricated fibers had uniform morphologies. The collected micrographs were analyzed to determine the fiber diameter distribution in each sample, and the resulting histograms are plotted in Fig. 1f. The blend fibers showed a relatively narrow distribution compared to PVDF fibers. Pure PCL had the smallest fiber diameter, and the average fiber diameter has grown as the PVDF content of the blend fibers has increased.

The bond structure of samples was assessed by FTIR spectroscopy, and the obtained spectra are shown in Fig. 2a. The characteristic bands of PCL appeared at 1722 and 1166 cm^{-1} due to C=O and C–O stretching vibrations, respectively. The carbon atoms belonging to the carbonyl group of PCL are known to interact with PVDF chains via hydrogen bonding; thus, the slightly blue-shifted C=O absorption band at 1725 cm^{-1} in all blend samples may be attributed to such interaction [33]. Furthermore, double bands at 2944 and 2866 cm^{-1} have emerged due to the symmetric and asymmetric stretching modes of CH_2 bonds in PCL [36]. The FTIR spectra of all electrospun composite fibers depicted the characteristic bands of PCL. The absorption lines at 510, 840, and 1274 cm^{-1} were evident in pure PVDF and all composite samples, and associated with the CF_2 bending, CH_2 rocking, and out-of-plane deformation of the C–F bond in polar β-phase PVDF, respectively [36,40–42]. The weak characteristic α-phase band at 763 cm^{-1} in the spectra indicates that PVDF is predominantly generated in β-phase chain conformation; nevertheless, the relative amounts of PVDF phases can be quantified using the unique absorption intensities for each phase in the FTIR spectra. The transmittance values provided in Fig. 2a can be used to calculate the absorbance data using the following equations.

$$A_\alpha = \log\left(\frac{I_\alpha^0}{I_\alpha}\right) \quad (1)$$

$$A_\beta = \log\left(\frac{I_\beta^0}{I_\beta}\right) \quad (2)$$

I^0 and I are the incident and transmitted beam intensities, respectively, and the α and β subscripts specify each phase. The absorption values at 763 and 840 cm^{-1} are specific to α and β structures, respectively. Incorporating the absorption data at these wave numbers into Eq. (3) gives the fraction of β-phase in PVDF [43,44].

$$F(\beta) = \frac{A_\beta}{1.26A_\alpha + A_\beta} \quad (3)$$

The fraction of the electroactive phase in the PVDF component and the entire composite was calculated, and results are plotted in Fig. 2b. As represented, the β-phase formation was predominant in samples with higher PVDF content. Of note, extending the β-PVDF chain conformation to larger fractions of the polymer requires intimate interactions

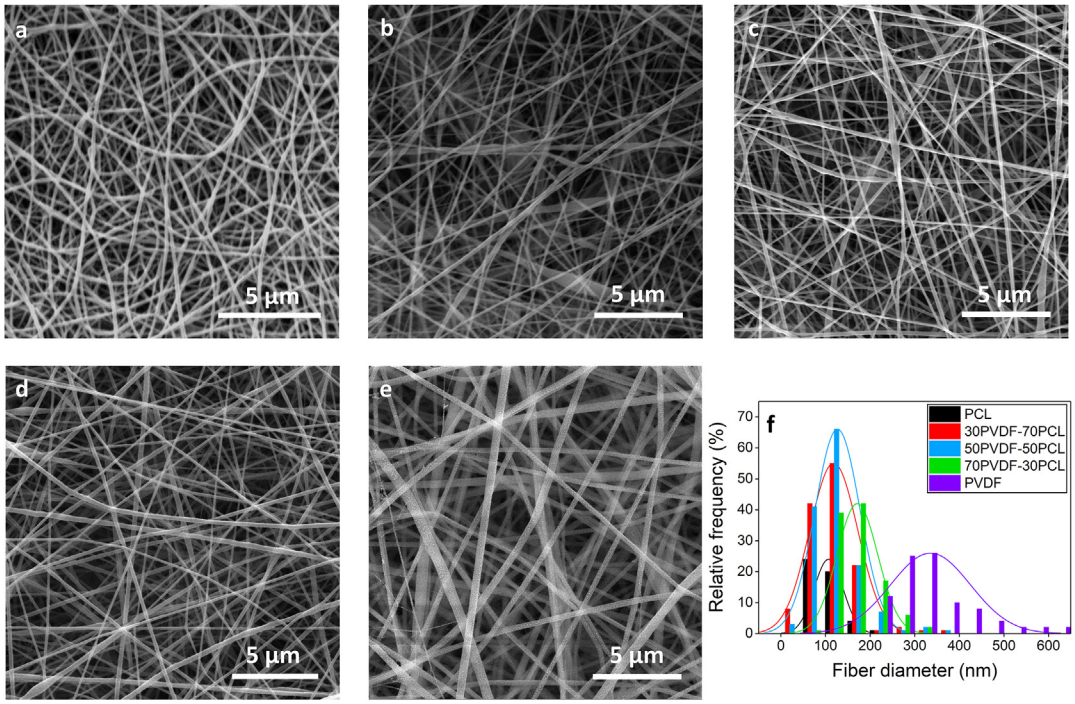

Fig. 1 – The morphology of electrospun fibers: a) PCL, b) 30PVDF-70PCL, c) 50PVDF-50PCL, d) 70PVDF-30PCL, e) PVDF, and f) fiber diameter distribution of electrospun fibers.

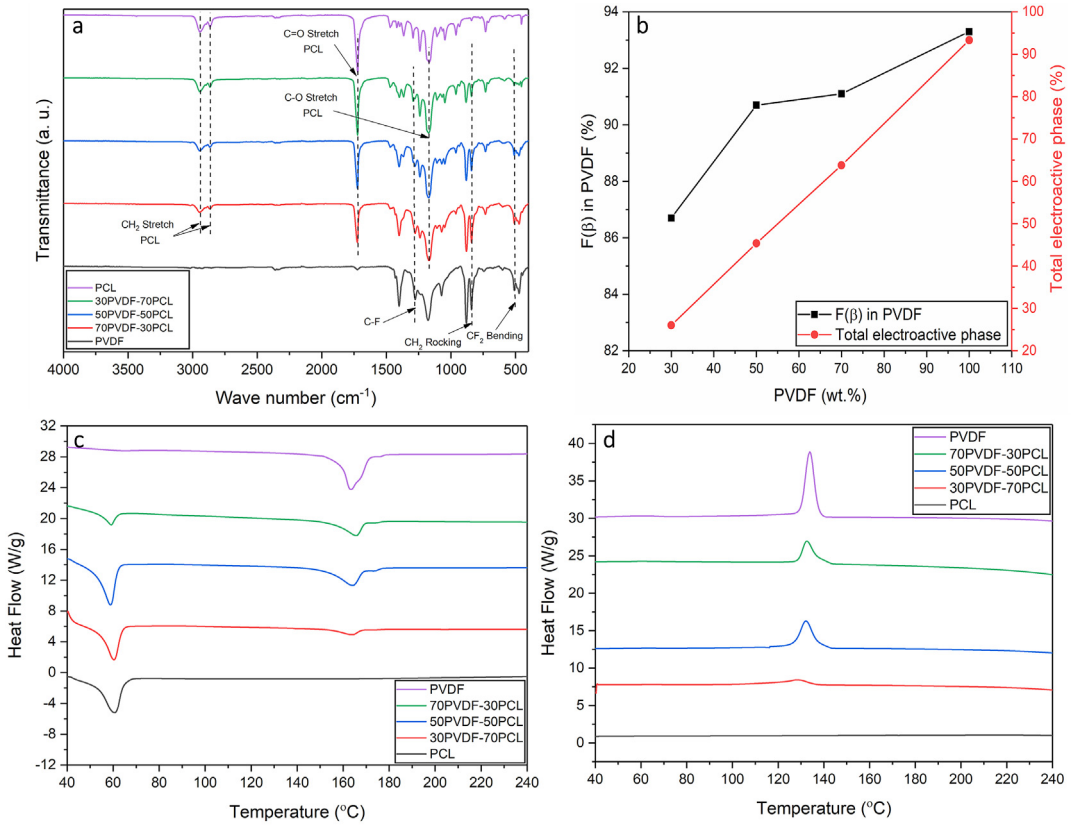

Fig. 2 – a) FTIR spectra of electrospun PVDF-PCL composites and their constituents, b) the variation of electroactive phases in the PVDF component and PVDF-PCL composites, c) DSC heating, and d) DSC cooling curves of electrospun PVDF-PCL fibrous samples and their pure components.

between PVDF polymer chains [45]. Further, the fraction of interfaces concerning the PVDF component grows as the overall PVDF content of the composite decreases; thus, the interface between PCL and PVDF affects a more significant portion of PVDF chains and restricts them from accommodating all-trans β-phase conformation. Consequently, low-content PVDF samples have a smaller β fraction.

To evaluate the thermal properties of materials and measure the crystallinity of the polymers, DSC was performed on all blend samples, and the obtained plots during the first heating and cooling cycles are presented in Fig. 2c and d, respectively. While the cooling cycle only provides information on the properties of the material, the heating cycle yields thermal properties associated with the fabrication process. Since electrospinning has a discernible impact on the phase structure and crystallinity of the polymers, the first heating cycle was analyzed and reported. The corresponding curves of pure PVDF and PCL electrospun fibers are also presented for better comparison.

In semicrystalline polymers, the enthalpy of melting can be used to estimate the crystallinity of the polymer using Eq. (4), where ΔH_m is the enthalpy of melting of the polymer, $\varnothing$ is the polymer fraction in a composite material, and ΔH_m^0 is the melting enthalpy of a fully crystalline polymer. The values of ΔH_m^0 for pure PVDF and PCL are reported as 104.7 and 139.5 J/g, respectively [28,46]. The enthalpy of melting for each polymer and the crystallinity percentage was calculated and presented in Table 1.

$$X_c = \frac{\Delta H_m / \varnothing}{\Delta H_m^0} \times 100 \quad (4)$$

The data given in Table 1 implies that the PCL crystallinity degree increases up to 50 wt% regarding the PVDF content, which is normally attributed to the difference in the melting temperature of these polymers when the fabrication method involves a heating stage. In such circumstances, the pre-

Table 1 – The obtained data from DSC plots of pure and blended electrospun samples. The o, m, and c indices denote onset, melting, and crystallization, respectively.

Sample Property	PCL	30PVDF-70PCL	50PVDF-50PCL	70PVDF-30PCL	PVDF
$T_{om,\ PVDF}$ (°C)	–	154.6	153.1	155.5	158.7
$T_{m,\ PVDF}$ (°C)	–	164.3	164.4	165.8	163.4
$\Delta H_{m,\ PVDF}$ (J/g)	–	32.61	39.22	41.41	41.61
$X_{c,\ PVDF}$ (%)	–	31.1	37.5	39.5	39.7
$T_{om,\ PCL}$ (°C)	52.4	54.2	51.7	53.3	–
$T_{m,\ PCL}$ (°C)	60.7	60.3	58.7	59.1	–
$\Delta H_{m,\ PCL}$ (J/g)	63.08	63.51	67.88	66.03	–
$X_{c,\ PCL}$ (%)	45.2	45.5	48.7	47.3	–
$T_{oc,\ PVDF}$ (°C)	–	136.3	137.8	138	137.6
$T_{c,\ PVDF}$ (°C)	–	128.2	132.2	132.6	133.9

crystallized PVDF component may prompt the PCL crystallization at about 50 °C; nevertheless, the explanation seems invalid here since both polymers had been dissolved in a solvent [32]. The initial concentrations of pure polymer solutions are likely the clue to this phenomenon. As noted earlier, the primary PVDF solution had a higher concentration and, thus, lesser solvent content than the PCL solution. Consequently, after blending solutions, the PVDF solvent would evaporate considerably faster; hence, PVDF crystallization precedes the PCL crystallization, and the pre-crystallized PVDF possibly plays the role of nucleating agent for the PCL component. Crystallization essentially occurs throughout the interfaces. As the relative proportion of interacting interfaces at 70 wt% is less than that of the 50 wt% PVDF-containing composites, the crystallinity of PCL declines; nevertheless, it is still significantly above that of pure PCL. Conversely, with increasing PCL concentration, the crystallinity of PVDF has declined, indicating that PCL cannot play the nucleating role for PVDF crystallization [47]. Moreover, the onset melting and crystallization temperatures of the PVDF were lower in all blend compositions compared to pure PVDF fibers. It is believed that the crystallization temperature is related to the crystal size. The decreasing crystallization trend shows that blending has induced confined crystallization in blend samples [33]. The melting temperature of the PCL component has the same behavior in the blend samples. These observations imply the existence of some degree of miscibility in the structure [32].

3.2. *Piezoelectric, surface, and mechanical properties*

The piezoelectric behavior of pure and blended polymer samples was assessed by the piezoelectric measurement device (Fig. 3a). Three fibrous samples of each composition were tapped 50 times by a load of 2 N at a frequency of 5 Hz. Upon loading, the output charge generated by samples was recorded by an oscilloscope (Fig. 3b). The alteration of the piezoelectric charge output according to the PVDF content is plotted in Fig. 3c. As represented, neat PCL is not piezoelectric; while in blend samples, the piezoelectric charge output has increased from 1.25 pC/N in 30PVDF-70PCL to 7.41 pC/N in 70PVDF-30PCL. Furthermore, the obtained results show a similar ascending trend with the fraction of the electroactive phase shown in Fig. 2b. The significant correlation observed between the PVDF content and piezoresponse in the prepared samples confirms that the relative β-phase fraction is mainly liable for the piezoelectricity of polymer blends. As was mentioned earlier, extending β-phase PVDF to larger portions of the polymer is impeded by the PVDF/PCL interface, which becomes more significant in low-content PVDF blend fibers. These changes in the structure directly affect the piezoelectric properties of the blend fibers. The polarization that occurred in β-phase PVDF upon tapping is responsible for the piezoelectric charge output. Therefore, Samples with more PVDF content, hence, higher β phase fraction, render greater piezoelectric output.

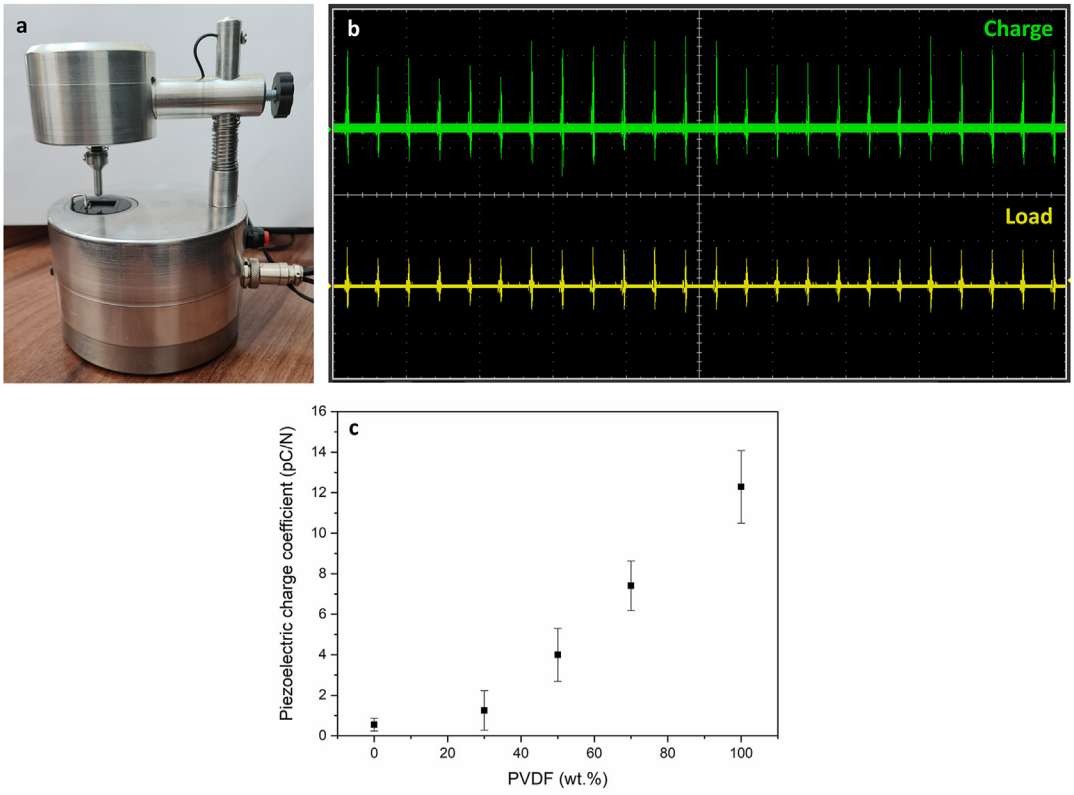

Fig. 3 – a) Piezoelectric measurement device, b) oscilloscope's screen of a piezoelectric sample, and c) piezoelectric response of pure PCL and PVDF and their blend electrospun fibers under a tapping load of 2 N at a frequency of 5 Hz.

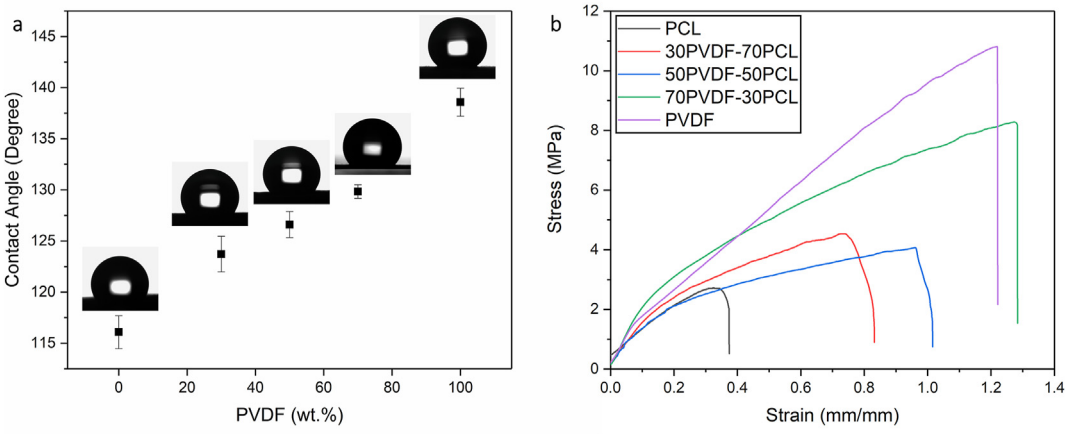

Fig. 4 – a) The water contact angle, and b) the stress-strain curves of pure PCL and PVDF, and their blend electrospun fibers.

Wettability is a crucial property in many applications where the material is exposed to water-based environments. The wettability of polymers greatly depends on the existing functional groups in their structure and their morphology. The water contact angle of the developed fibers was measured by a goniometer, and the results are presented in Fig. 4a. Since PCL is less hydrophobic, the water contact angle shows a descending trend with increasing PCL fraction in the polymer composites.

The mechanical performance of prepared fibers was assessed under tension. The related stress-strain curves are plotted in Fig. 4b, and the mechanical properties are presented in Table 2. Porous structures generally have lower mechanical strength and stiffness compared to bulk materials. For instance, bulk PCL samples have ultimate tensile strength (UTS) and Young's modulus of about 43 and 360 MPa, respectively [48]. Indeed, the increased surface area in the fibrous PCL structures comes at the expense of a dramatic decrease in mechanical properties. Herein, the fibrous PCL mat had a UTS of 2.44 MPa, which is within the lowest range of the reported UTS for bones [49]. Intriguingly, using PVDF in the blending approach improved the UTS value by almost 230% in the 70PVDF-30PCL sample. Meanwhile, the stiffness and elongation at break were significantly enhanced compared to pure PCL. These findings indicate that PVDF has a reinforcing effect on PCL mechanical properties in blend fibers. The applied force is transmitted onto the PVDF portion, which can effectively withstand larger applied stress, improving tensile strength. Moreover, PVDF with significant toughness can resist the propagation of crazes in the material. Therefore, blend fibers can undergo higher elongations. However, despite the increasing trend in tensile modulus, stiffness, and elongation at break with increasing PVDF, UTS has dropped in the sample containing 50 wt% of PVDF. The mechanical strength of multicomponent systems is deeply affected by the existence of interfaces. The 50PVDF-50PCL mat has the highest fraction of interfaces weakening the tensile strength of the material by restricting effective load transfer between the components. Once the detachment occurs at interfaces, the applied load cannot be transferred efficiently, leading to a drop in the tensile strength. Contrarily, the percent elongation is less prone to interfaces; meaning that upon interface detachment, the tougher portion of the material (PVDF in this case) can still elongate. As a consequence, the UTS has dropped in the 50PVDF-50PCL sample compared to 30PVDF-70PCL, but its elongation at break has increased.

Table 2 – The mechanical properties of PVDF/PCL fibers and their pure components.

Sample	Ultimate strength (MPa)	Elongation at break (%)	Tensile modulus (MPa)
PCL	2.44 ± 0.56	35.94 ± 6.19	8.89 ± 0.37
30PVDF-70PCL	4.18 ± 0.36	65.47 ± 8.49	12.95 ± 0.49
50PVDF-50PCL	3.43 ± 0.64	90.38 ± 5.82	14.55 ± 0.61
70PVDF-30PCL	8.28 ± 0.3	127.32 ± 1.67	21.54 ± 0.562
PVDF	11.65 ± 1.045	122.04 ± 8.5	18.95 ± 1.95

Regarding the surface properties of the fabricated samples, as well as their piezoelectric and mechanical properties, the 70PVDF-30PCL sample met the requirements for bone tissue engineering; thus, was considered for further biological studies in comparison to neat PVDF and PCL scaffolds.

3.3. *In-vitro biological and cell studies*

The metabolic activity of cells on PVDF, PCL, and blend PVDF/PCL fibers was evaluated by the Alamar blue assay and gathered data are represented in Fig. 5a. The meaningful increase in the metabolic activity in the presence of PVDF and PCL scaffolds (Fig. 5a) implies significant cell proliferation within 14 days. Contrarily, the obtained data showed no significant cell proliferation on the composite fibers in the same period. PCL is an FDA-approved biocompatible material; hence, the lack of daily difference among PVDF, 70PVDF-30PCL scaffolds, and PCL confirms that none of them had any cytotoxic effect for up to 14 days. Consistently, the picogreen assay data (Fig. 5b) confirm that all samples had approximately the same DNA content suggesting that their cell count is comparable to that of the control PCL group.

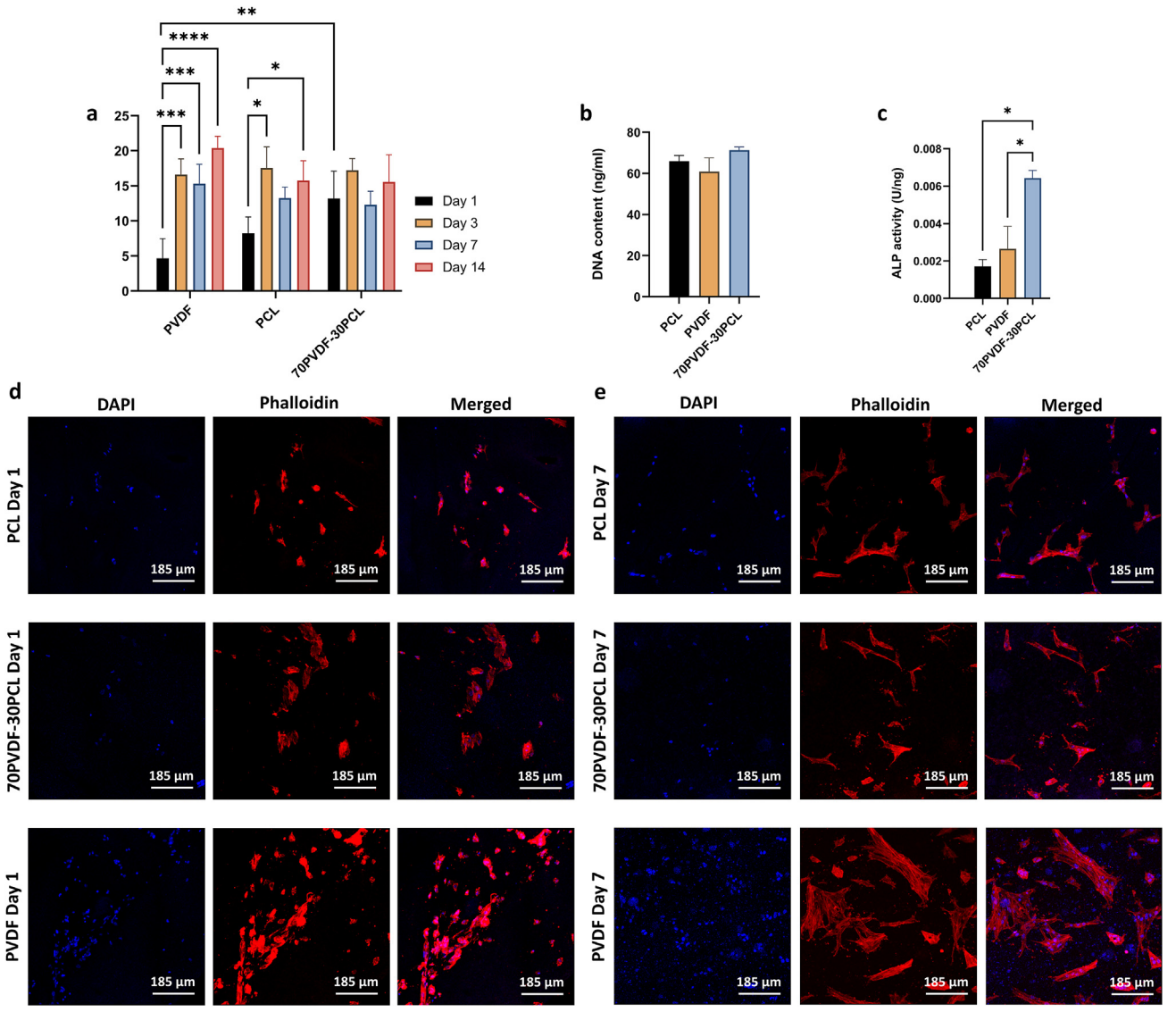

Fig. 5 – a) Alamar blue activity of hMSC cells for different experimental groups at 1, 3, 7, and 14 days. b) DNA content determined by Picogreen assay after 14 days. c) Quantification of ALP activity in cells on scaffolds at day 7. Representative confocal images of cells on scaffolds after 1 (d) and 7 (e) days. Actin filaments were stained with phalloidin (red) and cell nuclei with DAPI (blue). Error bars represent the standard deviation of three repetitions. *, $p < 0.05$; **, $p < 0.01$; ***, $p < 0.001$, and ****, $p < 0.0001$.

The ALP enzyme presents in numerous tissues, including bone, and has long been considered an early osteogenic differentiation marker [50]. Accordingly, the ability of the scaffolds to facilitate hMSCs differentiation into osteoblasts was investigated by examining the ALP function. The normalized ALP activity in cultured cells after 7 days is shown in Fig. 5c. The ALP activity in the presence of 70PVDF-30PCL was significantly higher compared to PVDF and PCL scaffolds. Further, the PVDF scaffold caused a slightly higher ALP induction than PCL. Notably, electromechanical stimulation has an established impact on osteogenic differentiation; therefore, PVDF and 70PVDF-30PCL scaffolds with remarkable piezoelectric properties would probably produce electromechanical stimulation upon cell attachment and migration [51]. Since the piezoelectric charge output is triggered by adhering cells to the scaffolds, their surface properties become critical. Morphology and wettability assessments showed that the 70PVDF-30PCL fibrous scaffold had a smaller average fiber diameter and water contact angle compared to the PVDF scaffold, facilitating cell attachment and migration on its surface. This agrees with the Alamar blue results, which showed nonsignificant cell proliferation on the 70PVDF-30PCL sample. Moreover, triggering differentiating pathways on the composite scaffold possibly provided chemical stimuli to stop cell proliferation [52].

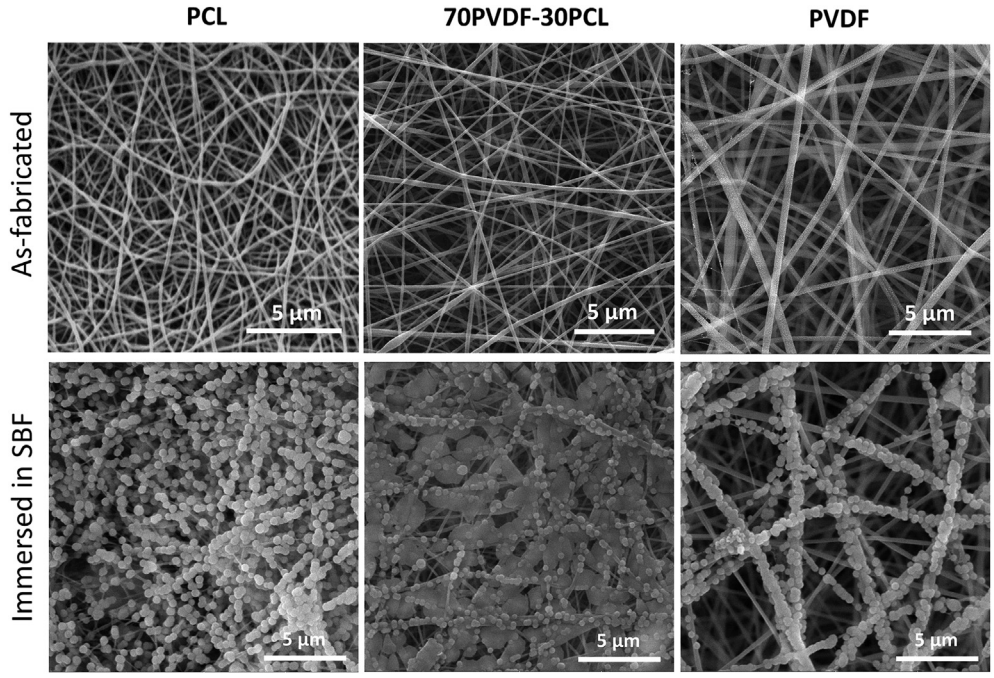

Fig. 6 – Apatite formation on the surface of electrospun fibers. The top row shows untreated samples, while the bottom row depicts samples immersed in SBF after 4 weeks.

The confocal images of actin (red) and nucleus (blue) staining after 1 and 7 days of cell culture are given in Fig. 5d and e, respectively. Stretching of actin filaments on day 7 compared to day 1 suggests that scaffolds have supplied a proper environment for cell attachment. Consistent with Alamar blue assay results, the increased number of blue-stained nuclei after one week in the presence of PVDF scaffold showed considerable cell proliferation, probably attributed to the electrical stimulation of cells. However, no remarkable cell proliferation was observed on 70PVDF-30PCL scaffolds, which was expected considering the Alamar blue and ALP activity assay results confirming the dominance of cell differentiation over proliferation in this sample.

To further understand the hierarchy of cellular activities augmentation due to the electric potential generated in response to mechanical loading in a piezoelectric biomaterial, it is worthwhile to look into the natural phenomenon in the bone tissue. Although the involving mechanisms in this process are not yet fully understood, researchers have found electrical stimulation responsible for improved bone adaptation and repair. It is believed that the electric potential could direct the activity of primary bone cells and also orient the arrangement of macromolecules in the natural bone ECM. Research studies in the mid-twentieth century speculated that osteocytes could detect high stress bone regions due to the higher electric potential in these areas [53]. Once cells migrated to the damaged bone site, further electromechanical stimulation would promote cell proliferation and also matrix mineralization of osteoblast-like cells. The underlying mechanism for the induced cell proliferation and differentiation in electrically stimulated zones is thought to be due to either the migration of intracellular components such as ions, growth factors, and receptors to these regions, which improves cellular activity or by the adsorption and conformation of extracellular ions and proteins onto the charged surface of the piezoelectric material [54]. Piezoelectric scaffolds can stimulate bone regeneration in almost the same manner by regulating calcium ionic pathways on cells membrane and inducing cell differentiation. Moreover, electrical stimulation could induce intracellular signaling by altering the polarization of cell membrane proteins, excelling cell migration towards the scaffold surface [55].

Bioactivity is another essential property of biomaterials recruiting in bone tissue engineering. Bone is continually remodeling due to its dynamic structure of organic nanofibers and calcium phosphate minerals [56]. Of note, the capacity of biomaterials to enable apatite structures generation on their surface is correlated with their bonding with living bone tissue, which can be evaluated by long-term soaking of biomaterials in the SBF solution [38]. Fig. 6 illustrates the morphology of the electrospun fibers after 4 weeks of soaking in SBF solution. Minerals precipitation has occurred in all samples. The morphology of the fibrous samples before immersion in SBF solution is also presented for a better comparison. As noted earlier, the PVDF scaffold has the highest average fiber diameter and thus the least surface area, leading to less precipitation, whereas the surface of the other two samples, with significantly thinner fibers and smaller pores, is almost entirely covered by the precipitated particles. Further, polar β-PVDF chains have well-separated negative and positive charge centers, disturbing the local dynamics of SBF and attracting the existing positive (Ca^{2+}) and negative (PO_4^{3-}) ions; however, these ions should be adsorbed on the surface of the fibers to form apatite nuclei. It is also worth mentioning that in-depth precipitation has not occurred in the PVDF scaffolds, probably due to the hydrophobic nature of the polymer and

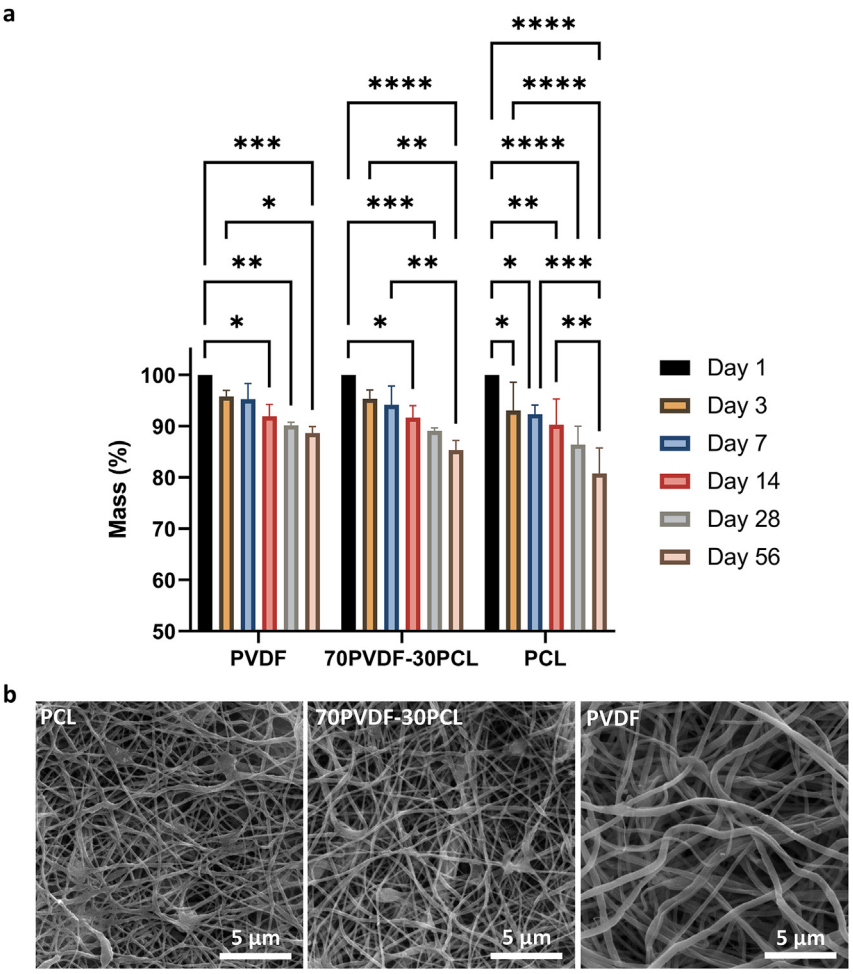

Fig. 7 – a) Biodegradation of the electrospun fibers in PBS within eight weeks, and b) electron micrographs of degraded samples after eight weeks.

limited SBF permeation into the scaffold [57]. In a nutshell, ion adsorption depends on the surface properties of the scaffolds. In the case of PVDF fibers, the smaller surface area and hydrophobicity have hindered proper ion adsorption and, thus, apatite formation. In contrast, a continuous apatite layer can be observed in the 70PVDF-30PCL sample, where surface properties and piezoelectricity favor mineral precipitation.

The biodegradation results of the electrospun samples in PBS medium within two months are represented in Fig. 7a. The morphology of samples after eight weeks of soaking in the PBS solution is also shown in Fig. 7b. The existing twisted and distorted fibers with thinned parts in SEM images can be regarded as evidence of biodegradation in the prepared scaffolds. For a better interpretation of the biodegradability results, meaningful differences were determined using two-way ANOVA analysis, and the obtained results are shown in Fig. 7a. The outcomes demonstrated that the samples' weight meaningfully decreased after two months in all five compositions. The PCL had a higher degradation rate in the PBS solution and lost 20% of its initial weight after two months. On the other hand, the PVDF degraded more slowly and retained about 90% of its initial mass at the end of the test period. As was expected, the presence of PCL has improved the biodegradation of polymer composites which is the consequence of a higher intrinsic degradation rate of PCL, the better wettability of composites containing higher PCL contents, and the presence of weak interfaces between PVDF and PCL portions.

Overall, the outcomes of the present research revealed that the PVDF/PCL blend electrospun fibers have significant piezoelectric performance, mainly due to the presence of the electroactive phase of PVDF. Intriguingly, the prepared degradable fibers showed good mechanical properties and were responsive to external stimuli to promote bone regeneration.

4. Conclusions

Regarding the research history, originating biocompatible scaffolds with optimized physicochemical characteristics facilitating the regeneration of bone defects is the main focus of investigations in this area. In the present study, a series of PVDF/PCL blends in the whole range of compositions were electrospun to produce fibrous scaffolds. The obtained data revealed that electrospinning could effectively induce β-

phase generation in the PVDF component. The evaluation of DSC heating and cooling profiles showed that PVDF regions could be the nucleating sites for PCL crystallization leading to an increased degree of crystallinity of PCL with PVDF percentage, up to a certain extent. Due to the development of the electroactive β phase in PVDF, the composite fibers became responsive to external loading and showed a piezoelectric response, positively correlated with PVDF content. While PCL showed almost zero piezoelectric performance, 70PVDF-30PCL rendered a piezoelectric charge output of about 7.5 pC/N. Further, blending PVDF with PCL improved wettability compared to pure PVDF; thus, these samples exhibited better biodegradability in PBS medium. In addition, the tensile test outcomes revealed that both the material composition and structure affect the mechanical properties of the scaffolds. Although PVDF addition to PCL would improve its mechanical performance, the extent of improvement would be less when the fraction of the weak interfacial region is relatively large, as in the 50PVDF-50PCL scaffold. In vitro cell studies showed that the 70PVDF-30PCL composite scaffold was biocompatible, and its piezoelectric response promoted stem cell differentiation into osteoblasts. According to the in vitro bioactivity results, apatite formation was observed in the prepared scaffolds, implying the suitability of the products for bone regeneration applications. Overall, the results showed that fibrous blended PVDF/PCL scaffolds with significant piezoelectric performance could be promising for scaffolds in bone tissue engineering.

Declaration of competing interest

The authors declare that they have no known competing financial interests or personal relationships that could have appeared to influence the work reported in this paper.

REFERENCES

[1] Dimitriou R, Jones E, McGonagle D, Giannoudis PV. Bone regeneration: current concepts and future directions. BMC Med 2011;9(1):1–10.

[2] Armiento AR, Hatt LP, Sanchez Rosenberg G, Thompson K, Stoddart MJ. Functional biomaterials for bone regeneration: a lesson in complex biology. Adv Funct Mater 2020;30(44):1909874.

[3] Abbasi N, Hamlet S, Love RM, Nguyen N-T. Porous scaffolds for bone regeneration. J Sci: advanced materials and devices 2020;5(1):1–9.

[4] Ogueri KS, Jafari T, Escobar Ivirico JL, Laurencin CT. Polymeric biomaterials for scaffold-based bone regenerative engineering. Regen Eng Trans Med 2019;5(2):128–54.

[5] Xie X, Chen Y, Wang X, Xu X, Shen Y, Aldalbahi A, et al. Electrospinning nanofiber scaffolds for soft and hard tissue regeneration. J Mater Sci Technol 2020;59:243–61.

[6] Chen Y, Dong X, Shafiq M, Myles G, Radacsi N, Mo X. Recent advancements on three-dimensional electrospun nanofiber scaffolds for tissue engineering. Advan Fiber Mater 2022:1–28.

[7] Khare D, Basu B, Dubey AK. Electrical stimulation and piezoelectric biomaterials for bone tissue engineering applications. Biomaterials 2020;258:120280.

[8] Bagheri B, Zarrintaj P, Samadi A, Zarrintaj R, Ganjali MR, Saeb MR, et al. Tissue engineering with electrospun electro-responsive chitosan-aniline oligomer/polyvinyl alcohol. Int J Biol Macromol 2020;147:160–9.

[9] Tandon B, Blaker JJ, Cartmell SH. Piezoelectric materials as stimulatory biomedical materials and scaffolds for bone repair. Acta Biomater 2018;73:1–20.

[10] Xu Q, Gao X, Zhao S, Liu YN, Zhang D, Zhou K, et al. Construction of bio-piezoelectric platforms: from structures and synthesis to applications. Adv Mater 2021;33(27):2008452.

[11] Ansari AA, Golebiowska A, Dash M, Kumar P, Jain PK, Nukavarapu S, et al. Engineering biomaterials to 3d-print scaffolds for bone regeneration: practical and theoretical consideration. Biomater Sci 2022;10:2789–816.

[12] Chen B, Lin Z, Saiding Q, Huang Y, Sun Y, Zhai X, et al. Enhancement of critical-sized bone defect regeneration by magnesium oxide-reinforced 3d scaffold with improved osteogenic and angiogenic properties. J Mater Sci Technol 2023:135 186–198.

[13] Yang X, Wang Y, Zhou Y, Chen J, Wan Q. The application of polycaprolactone in three-dimensional printing scaffolds for bone tissue engineering. Polymers 2021;13(16):2754.

[14] Dwivedi R, Kumar S, Pandey R, Mahajan A, Nandana D, Katti DS, et al. Polycaprolactone as biomaterial for bone scaffolds: review of literature. J Oral Bio Craniofac Res 2020;10(1):381–8.

[15] Siddiqui N, Kishori B, Rao S, Anjum M, Hemanth V, Das S, et al. Electropsun polycaprolactone fibres in bone tissue engineering: a review. Mol Biotechnol 2021;63(5):363–88.

[16] Deng R, Luo Z, Rao Z, Lin Z, Chen S, Zhou J, et al. Decellularized extracellular matrix containing electrospun fibers for nerve regeneration: a comparison between core–shell structured and preblended composites. Advan Fiber Mater 2022;4(3):503–19.

[17] Guastaferro M, Baldino L, Cardea S, Reverchon E. Supercritical processing of pcl and pcl-peg blends to produce improved pcl-based porous scaffolds. J Supercrit Fluids 2022;186:105611.

[18] Padalhin AR, Thuy Ba Linh N, Ki Min Y, Lee B-T. Evaluation of the cytocompatibility hemocompatibility in vivo bone tissue regenerating capability of different pcl blends. J Biomater Sci Polym Ed 2014;25(5):487–503.

[19] Zarrintaj P, Saeb MR, Jafari SH, Mozafari M. Application of compatibilized polymer blends in biomedical fields. Compatibilization of polymer blends; 2020. p. 511–37. Elsevier.

[20] Mishra S, Sahoo R, Unnikrishnan L, Ramadoss A, Mohanty S, Nayak SK. Enhanced structural and dielectric behaviour of pvdf-pla binary polymeric blend system. Mater Today Commun 2021;26:101958.

[21] Goonoo N, Bhaw-Luximon A. Piezoelectric polymeric scaffold materials as biomechanical cellular stimuli to enhance tissue regeneration. Mater Today Commun 2022:103491.

[22] Pusty M, Shirage PM. Insights and perspectives on graphene-pvdf based nanocomposite materials for harvesting mechanical energy. J Alloys Compd 2022:164060.

[23] Shoorangiz M, Sherafat Z, Bagherzadeh E. Cnt loaded pvdf-knn nanocomposite films with enhanced piezoelectric properties. Ceram Int 2022;48(11):15180–8.

[24] Faraz M, Singh HH, Khare N. A progressive strategy for harvesting mechanical energy using flexible pvdf-rgo-mos2 nanocomposites film-based piezoelectric nanogenerator. J Alloys Compd 2022;890:161840.

[25] Sabry RS, Hussein AD. Nanogenerator based on nanocomposites pvdf/zno with different concentrations. Mater Res Express 2019;6(10):105549.

[26] Ting Y, Chiu CW, Gunawan H. Characteristic analysis of biaxially stretched pvdf thin films. J Appl Polym Sci 2018;135(36):46677.
[27] Gomes J, Nunes JS, Sencadas V, Lanceros-Méndez S. Influence of the β-phase content and degree of crystallinity on the piezo-and ferroelectric properties of poly (vinylidene fluoride). Smart Mater Struct 2010;19(6):065010.
[28] Damaraju SM, Wu S, Jaffe M, Arinzeh TL. Structural changes in pvdf fibers due to electrospinning and its effect on biological function. Biomed Mater 2013;8(4):045007.
[29] Rasoolzadeh M, Sherafat Z, Vahedi M, Bagherzadeh E. Structure dependent piezoelectricity in electrospun pvdf-sic nanoenergy harvesters. J Alloys Compd 2022:165505.
[30] Rahmati M, Mills DK, Urbanska AM, Saeb MR, Venugopal JR, Ramakrishna S, et al. Electrospinning for tissue engineering applications. Prog Mater Sci 2021;117:100721.
[31] Jo WH, Park SJ, Kwon IH. Phase behavior of poly (ε-caprolactone)/poly (vinylidene fluoride) blends. Polym Int 1992;29(3):173–8.
[32] Kong Y, Ma Y, Lei L, Wang X, Wang H. Crystallization of poly (ε-caprolactone) in poly (vinylidene fluoride)/poly (ε-caprolactone) blend. Polymers 2017;9(2):42.
[33] Seraji SM, Guo Q. Polymorphism and crystallization in poly (vinylidene fluoride)/poly (ε-caprolactone)–block–poly (dimethylsiloxane)–block–poly (ε-caprolactone) blends. Polym Int 2020;69(2):173–83.
[34] Cheng Y, Xu Y, Qian Y, Chen X, Ouyang Y, Yuan W-E. 3d structured self-powered pvdf/pcl scaffolds for peripheral nerve regeneration. Nano Energy 2020;69:104411.
[35] Castkova K, Kastyl J, Sobola D, Petrus J, Stastna E, Riha D, et al. Structure–properties relationship of electrospun pvdf fibers. Nanomaterials 2020;10(6):1221.
[36] Hanumantharao SN, Alinezhadbalalami N, Kannan S, Friske M, Rao S. Electrospun acellular scaffolds for mimicking the natural anisotropy of the extracellular matrix. RSC Adv 2019;9(69):40190–5.
[37] Abazari MF, Soleimanifar F, Enderami SE, Nematzadeh M, Nasiri N, Nejati F, et al. Incorporated-bfgf polycaprolactone/polyvinylidene fluoride nanocomposite scaffold promotes human induced pluripotent stem cells osteogenic differentiation. J Cell Biochem 2019;120(10):16750–9.
[38] Kokubo T, Takadama H. How useful is sbf in predicting in vivo bone bioactivity? Biomaterials 2006;27(15):2907–15.
[39] Nagam Hanumantharao S, Rao S. Multi-functional electrospun nanofibers from polymer blends for scaffold tissue engineering. Fibers 2019;7(7):66.
[40] Szewczyk PK, Gradys A, Kim SK, Persano L, Marzec M, Kryshtal A, et al. Enhanced piezoelectricity of electrospun polyvinylidene fluoride fibers for energy harvesting. ACS Appl Mater Interfaces 2020;12(11):13575–83.
[41] Kalani S, Kohandani R, Bagherzadeh R. Flexible electrospun pvdf–batio 3 hybrid structure pressure sensor with enhanced efficiency. RSC Adv 2020;10(58):35090–8.
[42] Hernandez C, Gupta SK, Zuniga JP, Vidal J, Galvan R, Guzman H, et al. High pressure responsive luminescence of flexible eu3+ doped pvdf fibrous mats. J Mater Sci Technol 2021;66:103–11.
[43] Gebrekrstos A, Madras G, Bose S. Journey of electroactive β-polymorph of poly (vinylidenefluoride) from crystal growth to design to applications. Cryst Growth Des 2019;19(9):5441–56.
[44] Kim M, Fan J. Piezoelectric properties of three types of pvdf and zno nanofibrous composites. Advan Fiber Mater 2021;3(3):160–71.
[45] Martins P, Lopes A, Lanceros-Mendez S. Electroactive phases of poly (vinylidene fluoride): determination, processing and applications. Prog Polym Sci 2014;39(4):683–706.
[46] Wang X, Zhao H, Turng L-S, Li Q. Crystalline morphology of electrospun poly (ε-caprolactone)(pcl) nanofibers. Ind Eng Chem Res 2013;52(13):4939–49.
[47] Kim G-M, Le KHT, Giannitelli SM, Lee YJ, Rainer A, Trombetta M. Electrospinning of pcl/pvp blends for tissue engineering scaffolds. J Mater Sci Mater Med 2013;24(6):1425–42.
[48] Azevedo M, Reis R, Claase M, Grijpma D, Feijen J. Development and properties of polycaprolactone/hydroxyapatite composite biomaterials. J Mater Sci Mater Med 2003;14(2):103–7.
[49] Shkarina S, Shkarin R, Weinhardt V, Melnik E, Vacun G, Kluger PJ, et al. 3d biodegradable scaffolds of polycaprolactone with silicate-containing hydroxyapatite microparticles for bone tissue engineering: high-resolution tomography and in vitro study. Sci Rep 2018;8(1):1–13.
[50] Lee J-M, Kim M-G, Byun J-H, Kim G-C, Ro J-H, Hwang D-S, et al. The effect of biomechanical stimulation on osteoblast differentiation of human jaw periosteum-derived stem cells. Maxillofac Plast Reconst Surg 2017;39(1):1–9.
[51] Lee Y-S, Arinzeh TL. The influence of piezoelectric scaffolds on neural differentiation of human neural stem/progenitor cells. Tissue Eng 2012;18(19–20):2063–72.
[52] Marques-Almeida T, Cardoso VF, Gama M, Lanceros-Mendez S, Ribeiro C. Patterned piezoelectric scaffolds for osteogenic differentiation. Int J Mol Sci 2020;21(21):8352.
[53] Bassett CAL, Pawluk RJ, Becker RO. Effects of electric currents on bone in vivo. Nature 1964;204(4959):652–4.
[54] Mohammadkhah M, Marinkovic D, Zehn M, Checa S. A review on computer modeling of bone piezoelectricity and its application to bone adaptation and regeneration. Bone 2019;127:544–55.
[55] Shuai C, Liu G, Yang Y, Qi F, Peng S, Yang W, et al. A strawberry-like ag-decorated barium titanate enhances piezoelectric and antibacterial activities of polymer scaffold. Nano Energy 2020;74:104825.
[56] Samadian H, Mobasheri H, Azami M, Faridi-Majidi R. Osteoconductive and electroactive carbon nanofibers/hydroxyapatite nanocomposite tailored for bone tissue engineering: in vitro and in vivo studies. Sci Rep 2020;10(1):1–14.
[57] Malherbi MS, Dias LC, Lima MS, Ribeiro LG, Freitas VF, Bonadio TG, et al. Electrically stimulated bioactivity in hydroxyapatite/β-tricalcium phosphate/polyvinylidene fluoride biocomposites. J Mater Res Technol 2022;20:169–79.